Computing Illuminated Area and Scattering for Double-bounce for SAR Manmade Target's Characteristic Modeling

Kai Yang, Kefeng Ji, and Huanxin Zou
College of Electronics Science and Engineering, National University of Defense Technology
Changsha, Hunan 410073, China

Abstract— We take the perfect electrical conductor (PEC) dihedral with large dimension for example to analyze its double-bounce illumination cases for SAR manmade target's characteristic modeling. The completeness of the illumination cases is proved by rigorous mathematical reasoning and the range of the transmit aspect angle corresponding to each integral case is offered. The total scattering field is derived. Experiment results validate the dihedral's double-bounce scattering effect for each illumination case.

1. INTRODUCTION

SAR targets' scattering modeling is of great importance in SAR image interpretation. It can be derived by a variety of approaches. Model using physical optics (PO) maintains high computational efficiency and excellent accuracy under certain conditions. Double-bounce scattering effect can be found in a variety of manmade targets in real world scenes, such as ship-to-sea, vehicle-to-ground, building-to-ground, etc. [1–3]. However, determining the illuminated area of the double-bounce, as the primary task of this model, is very difficult. Thus, a complete solution to determine the illuminated area easily and accurately is derived in this paper.

Under the assumption of high-frequency and far field, we take the PEC dihedral with large dimension for example to analyze its double-bounce's illumination cases and find that there existed six classes of different integral(s) domain along with the transmit angle varying. Then the completeness of the illumination cases is proved by rigorous mathematical reasoning and the range of the transmit aspect angle corresponding to each integral case is also offered. Dihedral's double-bounce scattering effect corresponding to each integral case is computed based on PO integral equation. And combining the results of the double-bounce scattering effect with the single-bounce scattering, total scattering field of the right-angle dihedral is derived. Experiments validate these conclusions. And the proposed method can be extended to other scatterers whose scattering are dominated by double-bounce scattering effect.

2. ILLUMINATION CASES CALCULATION AND DEMONSTRATION

Reference 4 gives PO integral

$$\vec{E} = \frac{-jk\eta}{4\pi} \int\limits_S \hat{r} \times \left[\hat{r} \times \left(2\hat{n} \times \vec{H}_i\right)\right] e^{-jk\vec{r}'(\hat{k}_t - \hat{r})} dS \tag{1}$$

where k is the wavenumber, $k = 2\pi f/c$, η is the impedance, and $\sqrt{j} \equiv -1$. $\hat{r}$ is the receive direction, $\hat{n}$ is the unit vector norm to the surface S, $\vec{H}_i$ is the polarization of the incident magnetic field, $\vec{r}'$ is a vector from the origin to a point on the surface S, and k_t is the transmit direction.

Taking one step further, we can get

$$\vec{E} = -\frac{jk\eta}{4\pi} \left\{\hat{r} \times \left[\hat{r} \times \left(2\hat{n} \times \vec{H}_i\right)\right]\right\} \mathcal{I} \tag{2}$$

where $\mathcal{I} = \int_S e^{-jk\vec{r}'(\hat{k}_t - \hat{r})} dS$. Using formula (2), reference 5 gives the bistatic scattering solution for a rectangular plate. Employing the same manner, we can derive the total scattering solution for a right-angle dihedral. And the main task is how to calculate $\mathcal{I}$ for double-bounce.

2.1. Illumination Cases Analysis

Given the incident and scattered wave direction depicted in Figure 1, write them in Cartesian coordinates as

$$\hat{k}_t = -\left(\hat{x}\cos\phi_t \sin\theta_t + \hat{y}\sin\phi_t \sin\theta_t + \hat{z}\cos\theta_t\right) \tag{3}$$

$$\hat{r} = \hat{x}\cos\phi_r \sin\theta_r + \hat{y}\sin\phi_r \sin\theta_r + \hat{z}\cos\theta_r \tag{4}$$

The PEC right-angle dihedral is shown in Figure 2. Based on geometric optics (GO), we can get the single-bounce specular scattered wave direction, i.e., the double-bounce incident wave direction,

$$\hat{s}_{yz} = \hat{x}\cos\phi_t\sin\theta_t - \hat{y}\sin\phi_t\sin\theta_t - \hat{z}\cos\theta_t \tag{5}$$
$$\hat{s}_{xz} = -\hat{x}\cos\phi_t\sin\theta_t + \hat{y}\sin\phi_t\sin\theta_t - \hat{z}\cos\theta_t \tag{6}$$

where subscript denotes the plate reflected rays.

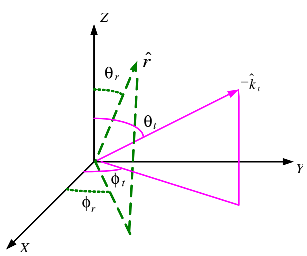

Figure 1: Bistatic spherical coordinate geometry.

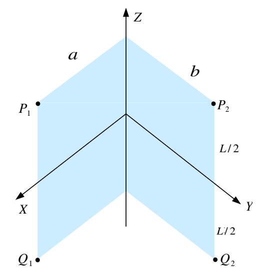

Figure 2: Right-angle dihedral.

From Figure 2, we get four corners coordinates: $P_1 = (a, 0, L/2)$, $Q_1 = (a, 0, -L/2)$, $P_2 = (0, b, L/2)$, $Q_2 = (0, b, -L/2)$. Based on space geometry, we can obtain the coordinates of the projections for four corners: $P_1' = (0,\ a\tan\phi_t,\ L/2 - a\cot\theta_t/\cos\phi_t)$, $Q_1' = (0,\ a\tan\phi_t,\ -L/2 - a\cot\theta_t/\cos\phi_t)$, $P_2' = (b\cot\phi_t,\ 0,\ L/2 - b\cot\theta_t/\sin\phi_t)$, $Q_2' = (b\cot\phi_t,\ 0,\ -L/2 - b\cot\theta_t/\sin\phi_t)$. Because of $0° \leq \phi_t \leq 90°$, we know that the projection points must be on the positive axis. If projection points, P_1', Q_1', are both on the plate, they must satisfy

$$\tan\phi_t \leq b/a \tag{7}$$

Similarly for P_2', Q_2', they must satisfy

$$\tan\phi_t \geq a/b \tag{8}$$

From formula (7) and (8), we can get

Conclusion 1: two set of projection points P_1', Q_1' and P_2', Q_2', are no more than one set on the plate.

On the other hand,

$$\left|P_1' - Q_1'\right| = \left|P_2' - Q_2'\right| = L \tag{9}$$

We have

Conclusion 2: P_1' and Q_1' are no more than one point on the plate, as same for P_2' and Q_2'.

From Conclusion 1 and 2, we can easily acquire

Conclusion 3: P_1', Q_1', P_2' and Q_2' are no more than one projection point on the plate.

If all four points aren't on the plate, there are two cases. One is that all four points are up the plate. The sufficient and necessary conditions of this case are

$$-b\cot\theta_t > L\sin\phi_t, \quad -a\cot\theta_t > L\cos\phi_t \tag{10}$$

The other case is all four points are down the plate. And the sufficient and necessary conditions are

$$b\cot\theta_t > L\sin\phi_t, \quad a\cot\theta_t > L\cos\phi_t \tag{11}$$

2.2. Illuminated Area Determination

Now, we know there are at least six illumination cases. Further analysis shows that there only exist six cases. Next, we prove the completeness of the six illumination cases by rigorous mathematical reasoning now.

Case 1: when P_1' is on the plate, the sufficient and necessary conditions are

$$0° \leq \theta_t \leq 90°, \quad \tan\phi_t \leq (b/a), \quad \cot\theta_t \leq (L/a)\cos\phi_t \tag{12}$$

Case 2: when P_2' is on the plate, the sufficient and necessary conditions are

$$0^\circ \leq \theta_t \leq 90^\circ, \quad \tan\phi_t \geq (b/a), \quad \cot\theta_t \leq (L/b)\sin\phi_t \tag{13}$$

Case 3: when all four points are down the plate, the sufficient and necessary conditions are formula (11).

Case4: when Q_1' is on the plate, the sufficient and necessary conditions are

$$90^\circ \leq \theta_t \leq 180^\circ, \quad \tan\phi_t \leq (b/a), \quad 0 \geq \cot\theta_t \geq -(L/a)\cos\phi_t \tag{14}$$

Case 5: when Q_2' is on the plate, the sufficient and necessary conditions are

$$90^\circ \leq \theta_t \leq 180^\circ, \quad \tan\phi_t \geq (b/a), \quad 0 \geq \cot\theta_t \geq -(L/b)\sin\phi_t \tag{15}$$

Case 6: when all four points are up the plate, the sufficient and necessary conditions are formula (10).

All these illumination cases are shown in Figure 3 respectively.

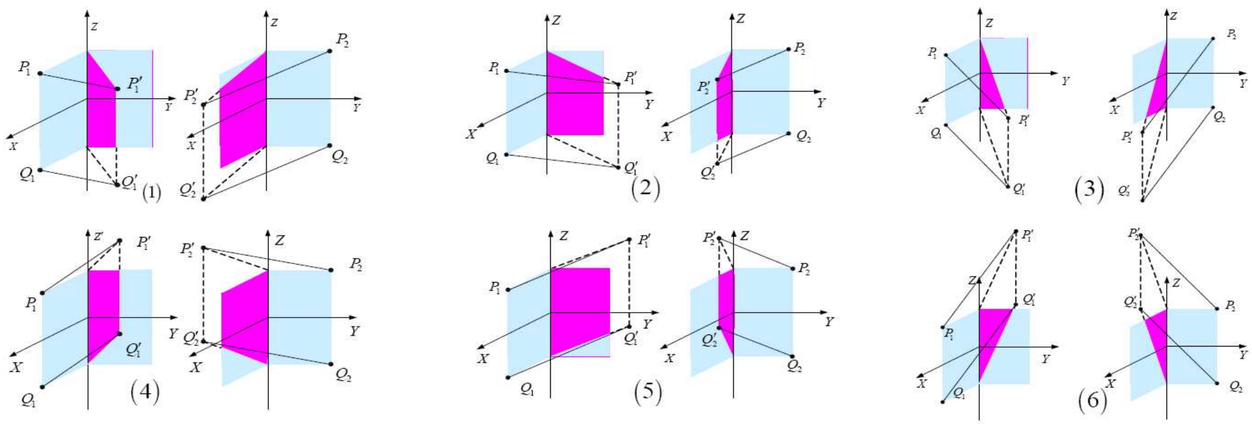

Figure 3: Illumination (illuminated area) of double-bounce for right-angle dihedral corresponding to illumination Cases 1–6.

Since Cases 4–6 are similar to Cases 1–3, now we just analyze the latter. The former can be done using the same manner. From Figure 3, we can see that there exist three cases for one plate of the dihedral, as shown in Figure 4. In the light of combination theory, there will be six cases existing.

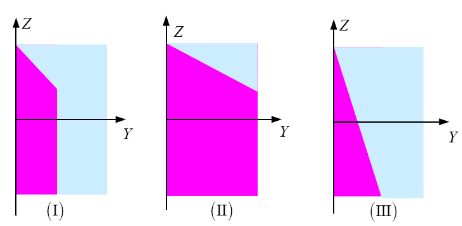

Figure 4: Illumination Cases (I)–(III) for one plate of the dihedral.

Now we analyze which case one plate is in when the other one (without loss of generality, we suppose it is yz plate) is in Case I. From Conclusion 1, we know that it is impossible for two plates both in Case I. The difference between the Cases II and III is the slope of the plate upper edge's projection. The bigger is for Case II, and the smaller is for Case III. We know that the slope of the plate's diagonal line is

$$k = -L/a \tag{16}$$

The slope of the projection line is

$$k' = -\cot\theta_t / \cos\phi_t \tag{17}$$

Since yz plate is in Case I, from formula (12), we know $k' \geq k$. Thus, this plate must be in Case II. Using the same analyzing manner, we have the following conclusions:

Conclusion 4: if one plate is in Case I, the other one must be in Case II.

Conclusion 5: if one plate is in Case II, the other one must be in Case I.

Conclusion 6: if one plate is in Case III, the other one also must be in Case III.

From Conclusions 4–6, we know that there just exist six illumination cases for right-angle dihedral for arbitrary transmit angles. The range of the transmit aspect angle corresponding to each illumination case are given in formula (10)–(15) respectively and illuminated area are shown in Figure 3.

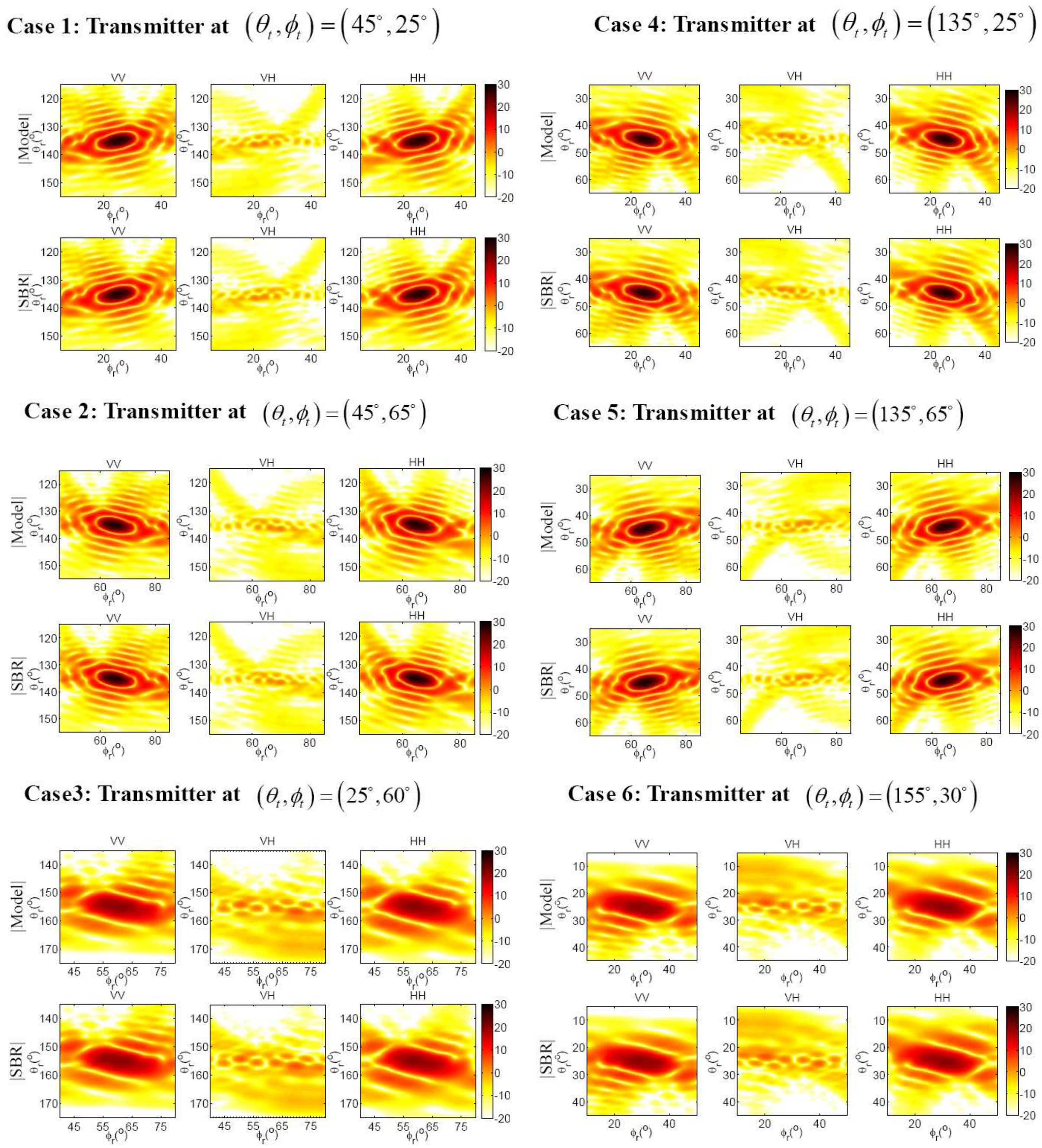

Figure 5: Comparison of bistatic dihedral polarization response for formula (19) and a shooting and bouncing rays prediction for six illumination cases.

3. SCATTERING FIELD CALCULATION

Section 2 analyzes illumination cases and gives the range of the transmit aspect angle corresponding to each illumination case. Thus, we can easily calculate $\mathcal{I} =$ for each illumination cases,

$$\begin{aligned}
\mathcal{I}_{xz}^{(1,2,3)} &= \frac{e^{j\frac{L}{2}\psi_z}}{j\psi_z} X\sin c\left(\frac{X}{2}\left(\psi_x+\frac{\cot\theta_t}{\cos\phi_t}\psi_z\right)\right)e^{-j\frac{X}{2}\left(\psi_x+\frac{\cot\theta_t}{\cos\phi_t}\psi_z\right)}-\frac{e^{-j\frac{L}{2}\psi_z}}{j\psi_z}X\sin c\left(\frac{X}{2}\psi_x\right)e^{-j\frac{X}{2}\psi_x}\\
\mathcal{I}_{yz}^{(1,2,3)} &= \frac{e^{j\frac{L}{2}\psi_z}}{j\psi_z} Y\sin c\left(\frac{Y}{2}\left(\psi_y+\frac{\cot\theta_t}{\cos\phi_t}\psi_z\right)\right)e^{-j\frac{Y}{2}\left(\psi_y+\frac{\cot\theta_t}{\sin\phi_t}\psi_z\right)}-\frac{e^{-j\frac{L}{2}\psi_z}}{j\psi_z}Y\sin c\left(\frac{Y}{2}\psi_y\right)e^{-j\frac{Y}{2}\psi_y}\\
\mathcal{I}_{xz}^{(4,5,6)} &= \frac{e^{j\frac{L}{2}\psi_z}}{j\psi_z} X\sin c\left(\frac{X}{2}\psi_x\right)e^{-j\frac{X}{2}\psi_x}-\frac{e^{-j\frac{L}{2}\psi_z}}{j\psi_z}X\sin c\left(\frac{X}{2}\left(\psi_x+\frac{\cot\theta_t}{\cos\phi_t}\psi_z\right)\right)e^{-j\frac{X}{2}\left(\psi_x+\frac{\cot\theta_t}{\cos\phi_t}\psi_z\right)}\\
\mathcal{I}_{yz}^{(4,5,6)} &= \frac{e^{j\frac{L}{2}\psi_z}}{j\psi_z} Y\sin c\left(\frac{Y}{2}\psi_y\right)e^{-j\frac{Y}{2}\psi_y}-\frac{e^{-j\frac{L}{2}\psi_z}}{j\psi_z}Y\sin c\left(\frac{Y}{2}\left(\psi_y+\frac{\cot\theta_t}{\sin\phi_t}\psi_z\right)\right)e^{-j\frac{Y}{2}\left(\psi_y+\frac{\cot\theta_t}{\sin\phi_t}\psi_z\right)}
\end{aligned}\tag{18}$$

where superscripts 1, 2, 3 and 4, 5, 6 indicate illumination Cases 1–3 and 4–6, respectively. And the subscripts xz and yz indicate the plate reflected rays. $\psi_x = k(\cos\phi_t\sin\theta_t - \cos\phi_r\sin\theta_r)$, $\psi_y = k(\sin\phi_t\sin\theta_t - \sin\phi_r\sin\theta_r)$, $\psi_z = k(\cos\theta_t + \cos\theta_r)$. And $X = b\cot\phi_t$, $Y = b$ for Cases 1, 4, $X = a$, $Y = a\tan\phi_t$ for Cases 2, 5, $X = L\tan\theta_t\cos\phi_t$, $Y = L\tan\theta_t\sin\phi_t$ for Case 3, and $X = -L\tan\theta_t\cos\phi_t$, $Y = -L\tan\theta_t\sin\phi_t$ for Case 6. Combining $\mathcal{I}$ with the result given by Reference 6, we obtain the bistatic 3D scattering solution for a right-angle dihedral,

$$\begin{aligned}
\vec{E}_{total} = \frac{jk}{2\pi}\Bigg\{&E_\theta\hat{\theta}_r\left[L\sin c\left(\frac{L}{2}\mathcal{Z}\right)\sin\theta_r\left(a\sin c\left(\frac{a}{2}\mathcal{X}\right)e^{\frac{ja}{2}\mathcal{X}}\sin\phi_t+b\sin c\left(\frac{b}{2}\mathcal{Y}\right)e^{\frac{jb}{2}\mathcal{Y}}\cos\phi_t\right)\right.\\
&\left.-\sin\theta_r(\mathcal{I}_{xz}\sin\phi_t+\mathcal{I}_{yz}\cos\phi_t)\right]-E_\phi\hat{\theta}_r\left[(\sin\theta_t\cos\theta_r\left(\mathcal{I}_{xz}\cos\phi_r-\ \mathcal{I}_{yz}\sin\phi_r\right)+\right.\\
&\sin\theta_r\cos\theta_t\left(\mathcal{I}_{xz}\cos\phi_t-\mathcal{I}_{yz}\sin\phi_t\right))+L\sin c\left(\frac{L}{2}\mathcal{Z}\right)\left[a\sin c\left(\frac{a}{2}\mathcal{X}\right)e^{\frac{ja}{2}\mathcal{X}}\ (\cos\theta_r\cos\phi_r\sin\theta_t\right.\\
&\left.\left.-\sin\theta_r\cos\theta_t\cos\phi_t)+b\sin c\left(\frac{b}{2}\mathcal{Y}\right)e^{\frac{jb}{2}\mathcal{Y}}\left(-\cos\theta_r\sin\phi_r\sin\theta_t\ +\sin\theta_r\cos\theta_t\sin\phi_t\right)\right]+\\
&E_\phi\hat{\phi}_r\left[L\sin c\left(\frac{L}{2}\mathcal{Z}\right)\sin\theta_t\left(a\sin c\left(\frac{a}{2}\mathcal{X}\right)e^{\frac{ja}{2}\mathcal{X}}\sin\phi_r+b\sin c\left(\frac{b}{2}\mathcal{Y}\right)e^{\frac{jb}{2}\mathcal{Y}}\cos\phi_r\right)\right.\\
&\left.+\sin\theta_t(\mathcal{I}_{xz}\sin\phi_r+\mathcal{I}_{yz}\cos\phi_r)\right]\Bigg\}
\end{aligned}\tag{19}$$

where $\mathcal{X} = k(\cos\phi_t\sin\theta_t + \cos\phi_r\sin\theta_r)$, $\mathcal{Y}=k(\sin\phi_t\sin\theta_t + \sin\phi_r\sin\theta_r)$, $\mathcal{Z} = k(\cos\theta_t + \cos\theta_r)$.

4. EXPERIMENTS

Six sets of experiments corresponded to six different illumination cases are done. The dimensions of the dihedral are $L = 1$, $a = 0.5$, $b = 0.5$. And the results shown in Figure 5 have excellent agreement with the SBR predictions. For easy comparison, formula (19) is organized into co/cross-pol scattering. V indicates vertical polarization (θ-pol), H indicates horizontal polarization (ϕ-pol), and the first script indicates receive polarization while the second script indicates transmitter polarization (HV polarization is omitted since the response is zero).

5. CONCLUSION

We take PEC dihedral with large size dimension for example to compute illuminated area and scattering for double-bounce for SAR manmade target's characteristic modeling. From results, we can see that what we derive shows excellent agreement with the SBR predictions. These indicate that the six illumination cases we derived are right and also mean that our method computing the illuminated area of dihedral is valid. Using the same method, we can compute illuminated area and scattering for double-bounce for other scatterers whose scattering are dominated by double-bounce scattering effect.

ACKNOWLEDGMENT

This work is supported by the National Natural Science Foundation of China under Grant 61372163, 61331015 and 61240058.

REFERENCES

1. Shepilko, Y. V., "Scattering of H-polarized electromagnetic wave by grooved dihedral wedge co-axially coupled with dielectric covered metal slotted cylinder," *2013 XVIIth International*

Seminar/Workshop on Direct and Inverse Problem of Electromagnetic and Acoustic (DIPED), 49–54, Sept. 23–26, 2013.

2. Tang, K., X. Sun, H. Sun, and H. Q. Wang, " A geometrical-based simulator for target recognition in high-resolution SAR images," *Geoscience and Remote Sensing Letters, IEEE*, Vol. 9, No. 5, 958–962, Sept. 2012.
3. Marble, J. A. and A. O. Hero, "See through the wall detection and classification of scattering primitives," *Proc. SPIE, Radar Sensor Technology X*, R. N. Trebits and J. L. Kurtz, Eds., Vol. 6210, 2006.
4. Knott, E. F., J. F. Shaeffer, and M. T. Tuley, *Radar Cross Section*, 2nd Edition, Artech House Boston, 1993.
5. Jackson, J. A., "Three-dimensional feature models for synthesis aperture radar and experiments in feature extraction," Ph.D. Dissertation, The Ohio State University, 2009.
6. Jackson, J. A., "Analytic physical optics solution for bistatic, 3D scattering from a dihedral corner reflector," *IEEE Transactions on Antennas and Propagation*, Vol. 60, No. 3, 1486–1495, 2012.